A Practical Countercurrent Fluid Catalytic Cracking Regenerator Model for In Situ Operation Optimization

Yongmin Zhang and Chunxi Lu
State Key Laboratory of Heavy Oil Processing, China University of Petroleum, Beijing 102249, P.R. China

Tingwen Li
URS Corp., Morgantown, WV 26505

DOI 10.1002/aic.12773
Published online October 14, 2011 in Wiley Online Library (wileyonlinelibrary.com).

A practical countercurrent fluid catalytic cracking (FCC) regenerator model with improved descriptions of gas and solid flow patterns is proposed. A three-zone and two-phase gas model was utilized to describe the gas flow through the regenerator, addressing the different phase mass-transfer properties in the different zones. A new two-continuously stirred-tank reactor-with-interchange model was used to describe the solid flow and to address the effect of freeboard on catalyst regeneration. Otherwise, this model also considered the usually adopted expanding section for reducing solid carryover. The model was programmed in Matlab language with coupled hydrodynamics and reaction kinetics models and tested and validated by the data from an industrial FCC regenerator operated under both partial and full CO combustion modes. After fitting a single model parameter, the interchange solid flux between the dense bed and freeboard, the model predictions were in reasonable agreement with the commercial data for both modes. © 2011 American Institute of Chemical Engineers
AIChE J, 58: 2770–2784, 2012
Keywords: regenerator, model, fluid catalytic cracking, fluidized bed

Introduction

A fluid catalytic cracking (FCC) unit is usually the workhorse of a modern petroleum refinery, which, aided by highly selective zeolite catalysts, cracks large-molecule low-value heavy oil feedstock into small-molecule high-value products, e.g., gasoline, diesel oil, and liquefied petroleum gas. For example, about 80 wt % gasoline, about 30 wt % diesel oil, and about 30 wt % propylene in China's market are produced by FCC process,[1] demonstrating its predominant role in petroleum refining industry. Reactor and regenerator are two indispensable parts of a typical FCC unit. A FCC reactor usually has a riser, a disengaging reactor, and a spent catalyst stripper, which is the place for desired catalytic cracking reactions. A regenerator is another indispensable part of a FCC unit, which burns the coke deposited on the spent catalyst and recovers its cracking activity. Mostly, a regenerator contains a single or multiple low-velocity fluidized beds operated under bubbling and turbulent regimes. However, there are some other types of fluidization regime utilized in FCC regenerators. For example, the UOP combustor-style FCC unit uses a fast bed to carry out the major duty of burning coke.[2]

Because of the widely used coke-sensitive zeolite catalyst in modern FCC units, a regenerator demands very low levels of carbon content in the regenerated catalyst (C_{Cr}) usually in the range of 0.05–0.1 wt % of catalyst weight. The carbon content in the spent catalyst is in the range of 1.0–1.5 wt % of catalyst weight. Therefore, as a solid-phase reactant, coke demands high conversion in a FCC regenerator. Furthermore, in view of the energy consumption and protection of catalyst activity in high-temperature steam atmosphere, a regenerator also requires minimized air consumption (usually oxygen content in the flue gas less than 3% in volume) and maximized coke burning intensity (CBI), which is usually defined as weight of coke burned for a given catalyst inventory in a given period, i.e.

$$\mathrm{CBI} = \frac{\text{weight of coke burned (kg)}}{\text{time (h)} \times \text{catalyst inventory (ton)}} \tag{1}$$

A higher CBI means a lower catalyst inventory and a shorter catalyst residence time in a regenerator, which means a lower rate of catalyst hydrothermal deactivation and a lower makeup rate for the fresh catalyst. It can thus be summarized that a high-efficiency regenerator is a noncatalytic gas–solid heterogeneous fluidized reactor with high demands for both gas and solid conversions.

Because of regenerator's self-explanatory importance for a FCC unit, modeling on catalyst regeneration process attracted a lot of attention from both academic researchers and industrial engineers. A practical regenerator model based on sound understanding of its intrinsic hydrodynamics, mixing, and reaction kinetics is undoubtedly helpful for optimizing the design and operation of FCC regenerators.

Correspondence concerning this article should be addressed to C. Lu at lcx725@sina.com.

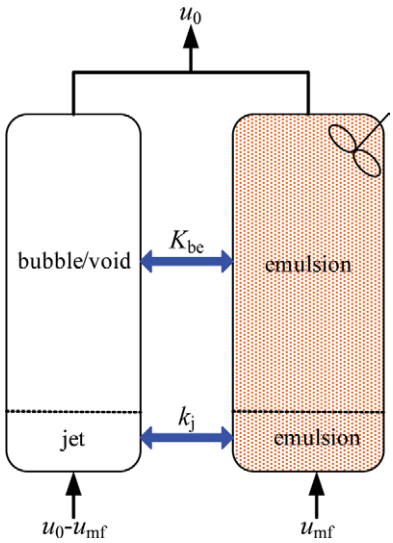

Figure 1. Schematic of the Orcutt model.[7]

[Color figure can be viewed in the online issue, which is available at wileyonlinelibrary.com.]

Despite various regenerators utilized in commercial FCC units, most of them, whether single-stage or two-stage regenerators, have at least a dense fluidized bed to maintain pressure balance and smooth particle circulation. This dense bed is usually operated at a superficial gas velocity range of 0.8–1.2 m/s, corresponding to a turbulent flow regime. Ford et al.[3] made the first attempt to model such a dense-bed regenerator with a one-phase pseudo-homogeneous model. This model omits the two-phase nature of the dense fluidized beds and the effect of freeboard. Therefore, it is too simple for precise modeling. The errors between modeled and measured oxygen contents in industrial regenerators were very large (in the range of −70% to 36%). De Lasa and coworkers[4-6] used a simple Orcutt model[7] to describe the gas flow and a continuously stirred-tank reactor (CSTR) model to describe the solid flow in the dense bed. Despite simple, their work represented the earliest attempts to use two-phase fluidized-bed models in FCC regenerators. They had examined the effects of various modeling assumptions on the development of industrial FCC regenerator models. Later, in similar manners, Faltsi-Saravelou et al.,[8] Filho et al.,[9] and Lu[10] modeled the FCC regenerators with different simplifications in the reaction kinetics or hydrodynamics. In these models, the grid zone (the region with a short distance above the distributor) was usually treated differently from the above bubbling zone for its much larger interphase mass-transfer rate. The study of Behie and Kehoe[11] showed that the interphase transfer rate can be 40–60 times higher than the bubbling zone. Therefore, distinguishing the grid and bubbling zone in the dense bed of a regenerator model is very necessary.

With bubbling and jet zones considered differently due to their large difference in interphase mass-transfer rate, the Orcutt-type regenerator model can be depicted schematically as Figure 1. Here, emulsion gas in both jet and bubbling zones is assumed to be in complete mixing, so gas reactant concentration in all emulsion regions of the dense bed is the same. In other words, although interphase mass-transfer rate in grid zone is far greater than in bubbling zone, reactant transferred from jet phase to the emulsion in the grid zone is still dispersed immediately into the remaining emulsion phase of the bubbling zone, maintaining a same reactant concentration. Therefore, if a same carbon content is assumed, the actual reaction rate in grid zone is the same as in bubbling zone. However, this is not consistent with experimental facts as found by Chavarie and Grace,[12] who found in their experiments that clear axial gradients of emulsion gas reactant concentration and reaction rate existed in the dense bed.

Guigon et al.[13] and Lee et al.[14] developed simple Kunii–Levenspiel[15] type models for FCC regenerators of various designs, where the gas reactant concentrations in the emulsion phase are proportional to those in the bubble phase, giving better agreement with the experimental facts. However, they did not consider the different rates of interphase mass transfer and reaction in the grid zone and freeboard, making their modeling results in question.

The efforts have also been made by McFarlane et al.,[16] Han and Chung,[17,18] Elnashaie et al.,[19] and Fernandes et al.[20] to model a whole FCC unit in dynamic- or steady-state modes. Different types of regenerator models were included in these models. However, these regenerator models were usually much simpler and just embedded in these complex FCC models, so their predicted results cannot be expected to be very agreeable with industrial data.

With the development of computational flow dynamics (CFD), attempts have been made to model the complex hydrodynamics and reactions in FCC regenerators, such as those of Schwarz and Lee[21] and Cao et al.[22] However, such fluidized-bed CFD models of Geldart Group A are very sensitive to mesh size.[23] The simulations of a large-dimensional industrial FCC regenerator with enough fine meshes are usually beyond the power of most current computers in the world. On the other hand, most current multiphase CFD codes are still under development and not fully mature yet. Grace and Taghipour[24] had pointed that all the current fluidized-bed CFD codes in the literature were in fact not fully verified or validated because of limited comparison between modeled and experimental results. Therefore, these models are at most valuable attempts and cannot be practical for guiding industrial design and operation.

Except for the need to consider the different mass-transfer rates in the grid zone, the role of freeboard in coke burning should be addressed in modeling a dense-bed regenerator. In a highly turbulent FCC regenerator, particles are frequently entrained into the freeboard due to vigorous movement of voids in the dense bed, resulting in a considerable solid fraction in the freeboard. According to Chen's estimations,[25] the solid inventory in the freeboard of an industrial FCC regenerator could be 20–35% of its total solid inventory. Moreover, the freeboard hydrodynamic characteristics are greatly different from that in the dense bed. Therefore, the effect of the freeboard on catalyst regeneration must not be neglected. De Lasa and Grace[4] proposed a model based on particle trajectories to calculate the coke burning in the freeboard, which assumed negligible mass-transfer resistance. In their model, rising and descending particles of different residence times and carbon contents were assumed, making this model too complex to be used in engineering practice. Lu[10] modeled the FCC regenerator freeboard by a multiple-CSTR-in-series model, with the number of CSTRs as an adjustable parameter. However, the modeled results of this model showed an overestimated temperature increase in the freeboard, greatly deviating from the measured data in industrial units and demonstrating a large discrepancy with the real solid flow patterns.

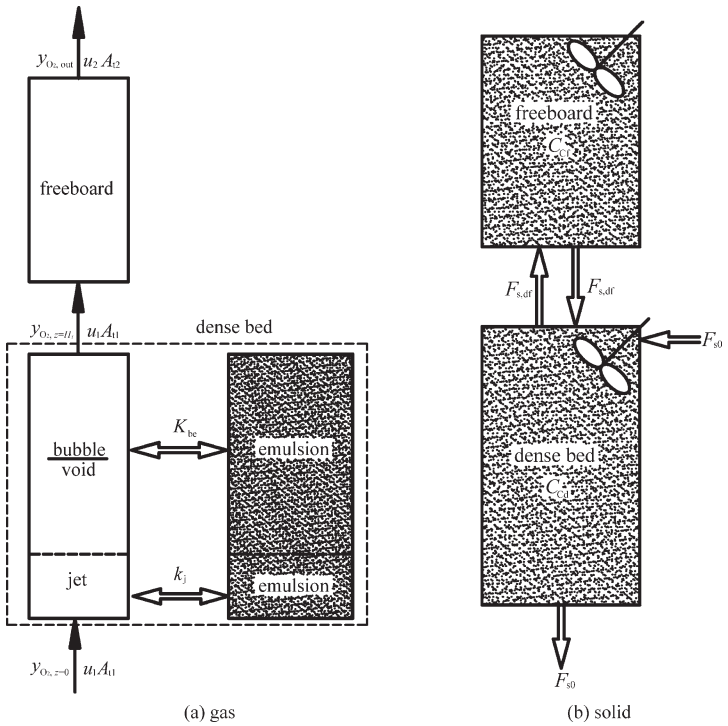

Figure 2. Gas and solid flow patterns in the countercurrent FCC regenerator model.

(a) Assumed gas flow pattern and (b) assumed solid flow pattern.

In summary, previous FCC regenerator models either used the Orcutt-type gas model with disagreeable axial emulsion gas concentration gradients with experimental facts, or did not fully consider the three zones (i.e., grid zone, bubbling zone, and freeboard) with different characteristics of mass transfer or hydrodynamic features, or too simple or complex to give practical guidance to industrial design and operation. The objective of this study is to establish a modified model for a countercurrent low-velocity regenerator widely used in FCC units. This model uses modified hydrodynamic models to provide better descriptions of gas and solid flows in both dense bed and freeboard. However, its structure still remains simple enough to make it a practical engineering tool. This model is designed as an operation-optimization tool. It needs the industrial data of a specific regenerator to determine its model parameters, but it can generate more detailed information of its performance, inner hydrodynamics and reactions than *in situ* measurements. In addition, it is capable of predicting the change of regeneration performance when operating variables change within a certain range of their previous operating points, thus guiding operators to reach optimized operating conditions.

Model Scheme

A countercurrent regenerator is usually a preferred choice in FCC units. In these regenerators, catalysts are injected near the dense bed surface, usually by a specially designed spent catalyst distributor, and withdrawn from the bottom of the dense bed. Therefore, catalysts flow from top to bottom, countercurrent contacting oxidizing gas (usually air) flowing from bottom to top. In countercurrent regenerators, lower-carbon-content catalysts contact with higher-oxygen-concentration air, whereas higher-carbon-content catalysts contact with lower-oxygen-concentration air, thus providing reasonably uniform carbon combustion rates and relatively high coke burning intensities throughout the bed.

As gas and solid (coke deposited in catalyst) are both involved in the reactions of catalyst regeneration, a FCC regenerator model needs to consider both gas and solid flow patterns. Figure 2 shows schematically the gas and solid flow patterns used in the current regenerator model. For gas flow in the dense bed, as shown in Figure 2a, a simple "two-phase bubbling bed model" proposed by Chavarie and Grace[12] is used. This model is a two-phase simplification of the three-phase Kunii and Levenspiel[15] model, which, as described previously, can provide better agreement with experiment data than the Orcutt model.[7] In this model, no gas flow exists in the emulsion phase due to the very small minimum fluidization velocity of FCC powders. Instead, gas in the emulsion phase is "stagnant." That is to say, gas reactants needed in reactions of emulsion phase can only be provided by interphase mass transfer. There is also no axial gas dispersion in the emulsion phase. For an irreversible first-order reaction A→B with no volume change, mole balances on A in the bubble and emulsion phases yield, respectively

$$u_0 \frac{dC_{Ab}}{dz} + k_{be}\alpha_b\delta_b(C_{Ab} - C_{Ae}) + k_r f_{sb} C_{Ab} = 0 \qquad (2)$$

and

$$k_{be}\alpha_b\delta_b(C_{Ae} - C_{Ab}) = k_r f_{se} C_{Ae} \qquad (3)$$

Along the height of the dense bed, the grid and bubbling zones have different mass-transfer rates, denoted by the symbols k_j and K_{be} in Figure 2a for the different interphase mass-transfer coefficients, respectively. In the grid zone, the dilute phase is composed of jets. The interphase mass-transfer rate could be much higher than in the bubbling zone, as much as 40–60 times higher according to the study of Behie

and Kehoe.[11] In the freeboard, the gas phase becomes a continuous phase, so the interphase mass-transfer resistance is negligible here. Reaction kinetics is then considered as the controlling factor. All gas flows in the three zones are assumed as plug flows without backmixing.

In industrial FCC regenerators, the axial solid dispersion coefficient in the dense bed was estimated to be about 1 m^2/s by van Deemter.[25] If the solid flow pattern is modeled by a tank-in-series model, its number of CSTR can be estimated by[26]

$$\frac{1}{N} = \frac{2}{Pe_s} - \frac{2}{Pe_s^2}(1 - \exp(-Pe_s)) \tag{4}$$

where Pe_s is the solid Peclet Number, i.e.

$$Pe_s = \frac{u_s H_f}{D_{a,s}}. \tag{5}$$

According to industrial data for superficial solid velocity u_s and bed height H_f, the estimated CSTR number N for a typical industrial dense-bed regenerator is very close to unity, so it is reasonable to model the dense bed as a CSTR as far as the solid flow is concerned.

Solids in freeboard originate mainly from particle entrainment due to bubble eruptions, i.e., from particles in the roofs and wakes of bubbles.[27] Solid concentration in freeboard decreases exponentially with increasing distance from the bed surface, demonstrating that the zone close to the bed surface, i.e., the so-called splash zone, contains the dominant fraction of solid inventory of the freeboard. Moreover, most particles rise and fall within a small height above the bed surface. Hence, there is a large solid exchange rate between the dense bed and the freeboard. For this reason, the multiple-CSTRs-in-series model used by Lu[10] underestimated the strong solid backmixing from freeboard to dense bed. Moreover, the strong turbulence induced by bubble eruptions, especially in the splash zone, can contribute to vigorous solid mixing. Based on the above analysis, the solid flow pattern is modeled in this model as two CSTRs with interchange.[26] Here, the dense bed and the freeboard are modeled as two CSTR reactors, respectively, as shown in Figure 2b. The function of the freeboard is to provide particles with additional time to burn coke with negligible interphase mass-transfer resistance. The periods spent by particles in the freeboard may vary from almost zero to a very long time, which is very similar to the residence time distribution in a typical CSTR reactor. Particles spent the longest period in the freeboard are those captured by cyclones and returned back to the dense bed by cyclone diplegs.

Other simplifications are used to facilitate the modeling. First, as showed in Figure 3, the hydrogen content of the coke is assumed to combust instantly at the bed surface. This results in an increase of gas flow rate by $u_{H_2O}A_{t1}$ because every mole of oxygen consumed produces 2 mol of water for the combustion of solid hydrogen component, as seen by the reaction equation: $4H(s) + O_2(g) \rightarrow 2H_2O(g)$. Otherwise, because of hydrogen combustion, a heat is inputted to the dense bed at $z = H_f$ as shown in Figure 3. In a countercurrent regenerator, spent catalyst is usually chosen to be sprayed into the dense bed near the bed surface by a spent catalyst distributor. The small mass-transfer resistance in the freeboard and the higher combustion rate of hydrogen[28] make the hydrogen in coke burn off very quickly. Although simple, this assumption is reasonable at least for countercurrent regenerators. Second, the structure of a typical FCC regenerator with an expanded freeboard is simplified as showed in Figure 3. The bottom bed section is always assumed to have the same height as the dense bed, H_f, whereas the expanded top section is assumed to be a cylinder of diameter d_{t2} and height $H_t - H_f$.

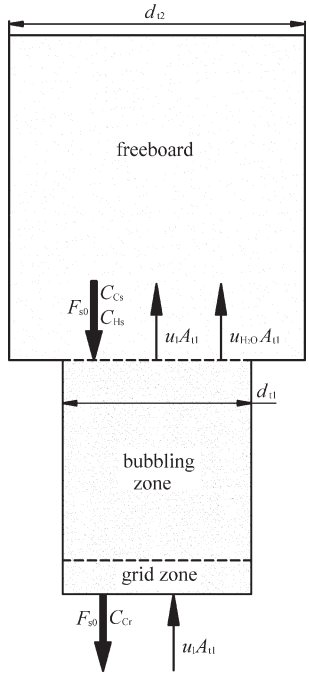

Figure 3. Simplified geometry model of a countercurrent FCC regenerator.

Except for the above simplifications, some other parameters in this model are also estimated based on existing industrial data, as introduced in the later sections. Because of this, the model can only be used to optimize the operation of existing FCC units. If used in newly designed units, there will be large errors in the modeled results.

Model Setup

Kinetics model

Because of the simplification for hydrogen combustion, only carbon combustion needs to be considered in this model. Carbon combustion can be described by

$$C + \frac{2\beta + 1}{2(\beta + 1)} O_2 \rightarrow \left(\frac{\beta}{\beta + 1}\right) CO_2 + \left(\frac{1}{\beta + 1}\right) CO \tag{6}$$

where β is the ratio of CO_2 to CO. The carbon combustion rate is estimated by

$$k_C = k_{C0} \exp\left(-\frac{E_C}{RT}\right) \tag{7}$$

Although a number of studies[29-32] have been conducted on the ratio of CO_2 to CO, it still remains difficult to estimate this ratio accurately. It is a function of a number of influencing factors such as catalyst type, feedstock, temperature, contents of oxygen in air, and CO promoters in catalyst. In this model, a simple method is used to determine the ratio of CO_2 to CO for each FCC unit, i.e.

$$\beta = \frac{y_{f,CO_2}}{y_{f,CO}} \tag{8}$$

where y_{f,CO_2} and $y_{f,CO}$ are the measured concentrations of CO_2 and CO in flue gas of an industrial regenerator under modeling. With this simplification, the actual combustion of CO, both homogeneously and heterogeneously, is greatly simplified.

Hydrodynamics model

Grid Zone. Two parameters are needed to model the hydrodynamics in the grid zone: jet length and jet diameter. In this model, jet length and jet diameter are both estimated by Lu's correlations[10]

$$L_j = 141.85 d_{or} \left(\frac{\rho_p d_p}{\rho_g d_{or}}\right)^{0.273} \left(\frac{\rho_g u_{or} d_{or}}{\mu_g}\right)^{-0.654} \left(\frac{u_{or}^2}{g d_{or}}\right)^{0.408} \tag{9}$$

$$D_j = 0.388 d_{or} \left(\frac{u_{or}^2}{g d_{or}}\right)^{0.332} \tag{10}$$

These two equations were correlated from experimental data in a large-scale (0.8 m I.D.) fluidized bed of FCC particles with a same type of sparger distributor as in industrial FCC units. The predicted jet length is taken as the height of the grid zone.

Bubbling Zone. The most important hydrodynamic parameter in the bubbling zone is the average bed density. Because of the large number of influencing factor involved, it is still difficult to date to find a generally applicable correlation. Here, a method based on the existing measured industrial data was proposed to estimate the bed density

$$\rho_B = \rho_{B,exp} + \frac{\partial \rho_B}{\partial u_1}(u_1 - u_{1e}) \tag{11}$$

where $\rho_{B,exp}$ and u_{1e} are the measured bed density and its corresponding operating gas velocity in a FCC regenerator, $\frac{\partial \rho_B}{\partial u_1}$ is the derivative of the bed density with respect to the superficial gas velocity, derived from the correlation of Cai et al.[33]

$$\varepsilon_B = G\left(\frac{Ly}{Ar}\right)^n \tag{12}$$

where $Ar = d_p^3 \rho_g (\rho_s - \rho_g) g / \mu_g^2$ is the Archimedes number, $Ly = u_0^3 \rho_g^2 \big/ (\rho_p - \rho_g) \mu_g g$ is the Lysenko Number, $n = 0.0653$, and $G = 0.796 + \frac{8.94 \times 10^{-3}}{d_t}$. Its derivative gives

$$\frac{\partial \rho_B}{\partial u_1} = \frac{\partial [\rho_p (1-\varepsilon)]}{\partial u_1} = -\frac{3n(\rho_p - \rho_{B,exp})}{u_1} \tag{13}$$

As there are usually small changes in operation parameters in optimizing industrial units, this method is expected to provide higher accuracies in the modeled results than by existing correlations. With average bed density known, other parameters in the bubbling zone, such as average bed voidage, bubble fraction, and bubble rise velocity, can be easily estimated as follows

$$\varepsilon_B = 1 - \frac{\rho_B}{\rho_p} \tag{14}$$

$$\delta_b = \frac{\varepsilon_B - \varepsilon_{mf}}{1 - \varepsilon_{mf}} \tag{15}$$

$$u_b = \frac{u_1}{\delta_b} \tag{16}$$

Dense Bed Height and Freeboard Solid Concentration Profile. Dense bed height and freeboard solid concentration profile are estimated by the method proposed by Zhang et al.[34] However, because of the existence of the expanded top sections in most industrial FCC regenerators, the original correlations need modification to calculate the corresponding parameters.

The solid fraction profile in the freeboard is assumed to follow the same empirical relationship as is represented in a single-diameter cylinder

$$f_s = f_s^* + \left(f_s^0 - f_s^*\right) \exp(-a z_f) \tag{17}$$

As a simplification, the saturated solid fraction f_s* is estimated by the measured inlet particle concentration in the first-stage cyclones

$$f_s^* = 1 - \frac{\rho_{in}}{\rho_p} \tag{18}$$

Because of the existence of the expanded freeboard section, the initial solid fraction f_s^0 is modified as

$$f_s^0 = \frac{0.3(u_1 - u_{mf})(1 - \varepsilon_{mf}) A_{t1}}{A_{t2} u_b} \tag{19}$$

with bubble rise velocity u_b estimated by Eq. 16.

The exponent coefficient α remains the same as in a single-diameter cylinder

$$a = \frac{0.7}{u_2} \tag{20}$$

A solid mass balance in the regenerator yields

$$\rho_B H_f A_{t1} + \rho_p A_{t2} \int_0^{H_t - H_f} f_s dz_f = M_s \tag{21}$$

where the bed height H_f is the only variable and hence can be calculated. With H_f determined, the solid concentration profile in the freeboard can thus be calculated. Hence, the solid inventory in the dense bed is

$$M_d = \rho_B A_{t1} H_f \tag{22}$$

and the solid inventory in the freeboard is

$$M_f = M_s - M_d \tag{23}$$

Interphase Mass-Transfer Coefficients. Mass-transfer coefficient between jet and emulsion is estimated by Lu's correlation[10] based on the data of Behie and Kehoe[11]

$$k_j = 0.48\left(\frac{d_{or}u_{or}\rho_{g,j}}{L_j}\right)\left(\frac{u_{or}^2}{gL_j}\right)^{-0.504}\left(\frac{L_j}{d_{or}}\right)^{0.905}\left(\frac{d_{or}u_{or}\rho_{g,j}}{u_{g,j}}\right)^{0.068} \quad (24)$$

Bubble-to-emulsion mass-transfer coefficient is estimated by the correlation of De Groot[35]

$$K_{be} = k_{be}a_b = \frac{u_1}{0.67H_f^{0.5}d_{t1}^{0.25}} \quad (25)$$

With this correlation, there is no need to know the average bubble size, which is very difficult to estimate, especially in large-scale industrial fluidized beds. Moreover, this correlation includes the effects of bed height and diameter.

Mass and heat balances

Oxygen Balance in the Dense Bed ($h \le H_f$*).* The oxygen concentration in the dense bed of a FCC regenerator is modeled by the "two-phase bubbling bed model" of Chavarie and Grace.[12] For simplification, the solid concentration in the dilute phases, i.e., bubble/void and jet phases, is assumed to be zero, and hence no reaction occurs in the dilute phases. Oxygen concentration can be represented as

$$-u_1\frac{dy_{b,O_2}}{dz} = \frac{k_j\alpha_{ji}A_ju_1}{M_AN_j}\left(y_{b,O_2} - y_{e,O_2}\right) \quad (26)$$

in the jet phase of the grid zone, whereas

$$\frac{k_j\alpha_{ji}A_ju_1}{M_AN_j}\left(y_{b,O_2} - y_{e,O_2}\right) = K_{dr}y_{e,O_2} \quad (27)$$

in the emulsion phase of the grid zone. Here, K_{dr} is the reaction constant in the emulsion phase of the dense bed defined as

$$K_{dr} = \frac{2\beta+1}{2(\beta+1)}k_CC_{Cd}(P_t + \rho_BH_fg/2)\rho_BV_{md} \quad (28)$$

where V_{md} is the mole volume in the dense bed

$$V_{md} = 22.4\frac{P_NT_d}{P_dT_N} \quad (29)$$

In the void phase of the bubbling zone, a mole balance gives

$$-u_1\frac{dy_{b,O_2}}{dz} = \delta_bK_{be}\left(y_{b,O_2} - y_{e,O_2}\right) \quad (30)$$

whereas

$$\delta_bK_{be}\left(y_{b,O_2} - y_{e,O_2}\right) = K_{dr}y_{e,O_2} \quad (31)$$

in the emulsion phase of the bubbling zone.

With two mass-transfer constants

$$K_{dj} = \frac{k_j\alpha_{ji}A_ju_1}{M_AN_j} \quad (32)$$

$$K_{db} = \delta_bK_{be} \quad (33)$$

defined in the grid and bubbling zones, respectively, the oxygen concentration in the dense bed can be predicted

$$y_{b,O_2,z=h} = y_{b,O_2,z=0}\exp\left[-\frac{K_{dj}K_{dr}h}{u_1\left(K_{dr}+K_{dj}\right)}\right] \quad (34)$$

$$y_{e,O_2,z=h} = \frac{K_{dj}y_{b,O_2,z=h}}{K_{dr}+K_{dj}} \quad (35)$$

in the grid zone ($h \le L_j$) and

$$y_{b,O_2,z=h} = y_{b,O_2,z=L_j}\exp\left[-\frac{K_{dr}K_{db}}{u_1(K_{dr}+K_{db})}\left(h-L_j\right)\right] \quad (36)$$

$$y_{e,O_2,z=h} = \frac{K_{db}y_{b,O_2,z=h}}{K_{dr}+K_{db}} \quad (37)$$

in the bubbling zone ($L_j \le h \le H_t$).

Oxygen Balance in Freeboard ($H_f \le h \le H_t$*).* In the freeboard, interphase mass transfer is neglected, with reaction kinetics viewed as the controlling factor, so the oxygen concentration is given by

$$-u_2\frac{dy_{O_2}}{dz} = \frac{2\beta+1}{2(\beta+1)}k_CC_{Cf}\rho_fP_ty_{O_2}V_{mf} \quad (38)$$

where ρ_f is the freeboard particle concentration, calculated by Eq. 17. Equation 38 can be integrated to give

$$y_{O_2,z=h} = y_{O_2,z=H_f}\exp\left\{-\frac{K_{fr}f_s^*(h-H_f)}{u_2} - K_{fr}\left(f_s^0 - f_s^*\right)\frac{[1-\exp(\alpha H_f - \alpha h)]}{\alpha u_2}\right\} \quad (39)$$

where K_{fr} is the reaction constant defined for the freeboard

$$K_{fr} = \frac{2\beta+1}{2(\beta+1)}k_CC_{Cf}\rho_pP_tV_{mf} \quad (40)$$

Concentration Profiles of CO_2 and CO. With the oxygen concentration profile known, the concentrations of CO_2 and CO at a given height can be obtained from

$$y_{CO_2,z=h} = \frac{2\beta}{2\beta+1}\left(y_{O_2,z=0} - y_{O_2,z=h}\right) \quad (41)$$

$$y_{CO,z=h} = \frac{2}{2\beta+1}\left(y_{O_2,z=0} - y_{O_2,z=h}\right) \quad (42)$$

Carbon Balance. The carbon balance in the dense bed can be represented schematically in Figure 4, where rCd represents the carbon loss rate due to carbon combustion, expressed by

$$\frac{F_{s0}(C_{Cs} - C_{Cd})}{100} = \frac{F_{s,df}(C_{Cd} - C_{Cf})}{100} + 12N_{dt}\left(y_{CO_2,z=H_f} + y_{CO,z=H_f}\right) \quad (43)$$

Here, r_{Cd} equals to the right second item of Eq. 43. The carbon balance in the freeboard, as shown in Figure 5, can be expressed by

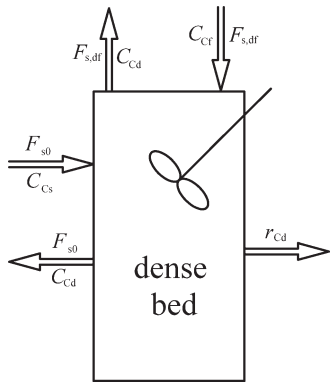

Figure 4. Carbon balance in the dense bed.

$$\frac{F_{s,df}(C_{Cd}-C_{Cf})}{100}=12N_{ft}\left[\left(y_{CO_2,z=H_t}-y_{CO_2,z=H_f}\right)+\left(y_{CO,z=H_t}-y_{CO,z=H_f}\right)\right] \quad (44)$$

Combining Eqs. 43 and 44 yields

$$C_{Cd}=C_{Cs}-\frac{1200N_{ft}}{F_{s0}}\left(y_{CO_2,z=H_t}+y_{CO,z=H_t}\right) \quad (45)$$

With C_{Cd} known, C_{Cf} can then be predicted by Eq. 43 as

$$C_{Cf}=C_{Cd}-\frac{1200N_{ft}}{F_{s,df}}\left[\left(y_{CO_2,z=H_t}-y_{CO_2,z=H_f^+}\right)+\left(y_{CO,z=H_t}-y_{CO,z=H_f^+}\right)\right] \quad (46)$$

Heat Balance. The heat balance in the dense bed, depicted in Figure 6, includes the following terms:

(1) Heat input due to carbon combustion Q_{dr1}

$$Q_{dr1}=12N_{dt}\left(\Delta H_{CO_2}y_{CO_2,z=H_f}+\Delta H_{CO}y_{CO,z=H_f}\right) \quad (47)$$

(2) Heat input due to hydrogen combustion Q_{dr2}

$$Q_{dr2}=0.7\Delta H_{H_2O}F_{s0}C_{Hs} \quad (48)$$

(3) Heat input due to particle circulation between the dense bed and the freeboard, $F_{s,df}C_{ps}(T_f-T_d)$.

(4) Sensible heat gain by catalyst, $F_{s0}C_{ps}(T_d-T_s)$.

(5) Sensible heat gain by flowing gas, $u_1A_{t1}\rho_gC_{pg}(T_d-T_0)$.

(6) Coke desorption heat, Q_{dd}, calculated by the following correlation[36]

$$Q_{dd}=0.057(Q_{dr1}+Q_{dr2}) \quad (49)$$

(7) Heat loss from the outside shell, Q_{dl}, estimated by the same method used as in Lu's model[10]

$$Q_{dl}=3.135\pi d_{t1}H_f \quad (50)$$

(8) Heat loss due to removal by catalyst coolers (often used in resid FCC units to remove the residue regeneration heat to maintain the heat balance of FCC units), Q_{dc}, which is an input variable in this model.

The overall heat balance is then

$$Q_{dr1}+Q_{dr2}+F_{s,df}C_{ps}(T_f-T_d)=F_{s0}C_{ps}(T_d-T_s)+u_1A_{t1}\rho_gC_{pg}(T_d-T_0)+Q_{dd}+Q_{dl}+Q_{dc} \quad (51)$$

By defining

$$Q_{Cd}=(Q_{dr1}+Q_{dr2})-(Q_{dd}+Q_{dl}+Q_{dc}) \quad (52)$$

and

$$B_{Cd}=F_{s0}C_{ps}+u_1A_{t1}\rho_gC_{pg} \quad (53)$$

Eq. 51 can be simplified as

$$Q_{Cd}+F_{s,df}C_{ps}(T_f-T_d)=B_{Cd}T_d-F_{s0}C_{ps}T_s-u_1A_{t1}\rho_gC_{pg}T_0 \quad (54)$$

Similarly, the heat balance in the freeboard, as depicted in Figure 7, includes the following terms:

(1) Heat input due to carbon combustion Q_{fr1}

$$Q_{fr1}=12N_{ft}\left[\Delta H_{CO_2}\left(y_{CO_2,z=H_t}-y_{CO_2,z=H_f}\right)+12\Delta H_{CO}\left(y_{CO,z=H_t}-y_{CO,z=H_f}\right)\right] \quad (55)$$

(2) Heat input due to hydrogen combustion Q_{fr2}

$$Q_{fr2}=0.3\Delta H_{H_2O}F_{s0}C_{Hs} \quad (56)$$

(3) Sensible heat loss due to particle circulation between the dense bed and the freeboard, $F_{s,df}C_{ps}(T_f-T_d)$.

(4) Sensible heat gain due to gas flow, $u_1A_{t1}\rho_gC_{pg}(T_f-T_d)$.

(5) Coke desorption heat Q_{fd}

$$Q_{fd}=0.057(Q_{fr1}+Q_{fr2}); \quad (57)$$

(6) Heat loss from outside shell Q_{fl}

$$Q_{fl}=3.135\pi d_{t2}(H_t-H_f). \quad (58)$$

The overall heat balance is then

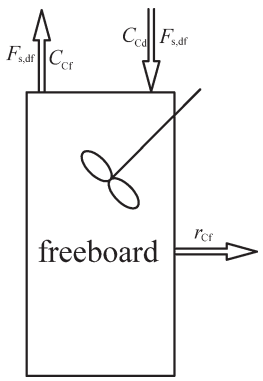

Figure 5. Carbon balance in the freeboard.

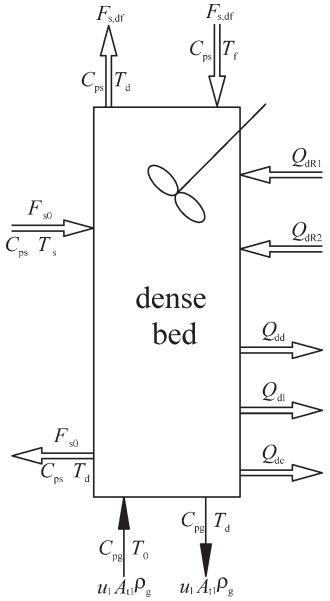

Figure 6. Heat balance in the dense bed.

$$Q_{fr1} + Q_{fr2} = F_{s,df}C_{ps}(T_f - T_d) + u_2A_{t2}\rho_g C_{pg}(T_f - T_d) + Q_{fd} + Q_{fl} \quad (59)$$

By defining

$$Q_{Cf} = (Q_{fr1} + Q_{fr2}) - (Q_{fd} + Q_{fl}) \quad (60)$$

and

$$B_{Cf} = F_{s,df}C_{ps} + u_2A_{t2}\rho_g C_{pg} \quad (61)$$

Eq. 59 can be simplified as

$$Q_{Cf} = B_{Cf}(T_f - T_d) \quad (62)$$

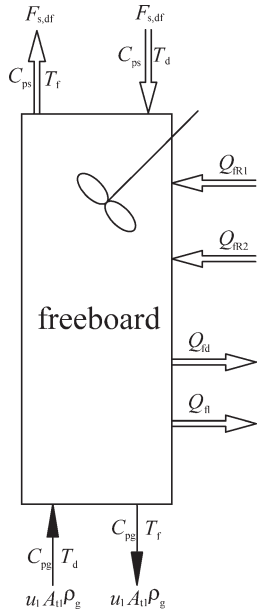

Figure 7. Heat balance in the freeboard.

Substituting Eq. 62 into Eq. 59 gives

$$T_d = \frac{\left(Q_{Cd} + F_{s,df}C_{ps}\frac{Q_{Cf}}{B_{Cf}} + F_{s0}C_{ps}T_s + u_1A_{t1}\rho_g C_{pg}T_0\right)}{B_{Cd}} \quad (63)$$

The freeboard temperature can then be calculated from Eq. 62, giving

$$T_f = T_d + \frac{Q_{Cf}}{B_{Cf}} \quad (64)$$

Solution Algorithm. All the simplifications regarding to hydrodynamics, reactions and kinetics, and reactor geometry as well as their associated effects on modeling are summarized in Table 1.

This model is programmed in Matlab language using a modularized scheme and solved by an iterative method as shown in Figure 8. There are seven modules and two iteration loops. To establish a model for optimizing the operation of a specified FCC regenerator, a calibration procedure is required to determine the key unit-dependent parameters based on existing industrial data. After that, basic operating parameters can be changed to see their effects on the performance of the regenerator and to determine optimized operating parameters.

The seven main modules in this program are raw data, data initialization, hydrodynamics, gas component balance, carbon balance, heat balance, and output. The raw data module is used to store the industrial data for a specified FCC regenerator under modeling. In the data initialization module, some basic calculations are carried out, such as the calculation of superficial gas velocities. During the process of determining unit-dependent parameters, these calculations are based on the raw data. However, some basic operating data can be changed during optimizations to see their effects on the performance of the regenerator. The hydrodynamic parameters as listed in section "Mass and Heat Balance" are then calculated in the hydrodynamics module. After these data pretreatments, initial values of C_{Cd}, C_{Cf}, T_d, and T_f are set first. With these initial values, the concentration profiles of oxygen, CO_2, and CO can be determined by the gas component balance module, and new values of C_{Cd} and C_{Cd}

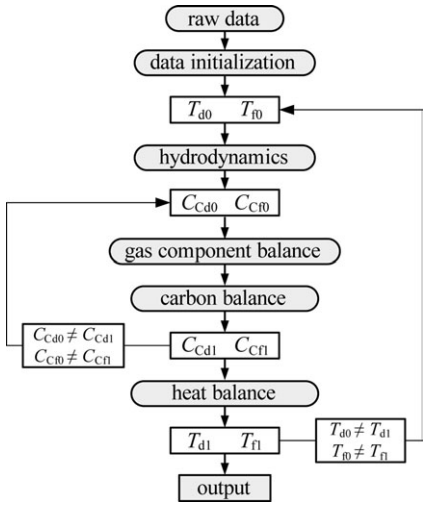

Figure 8. Flow chart of model program.

Table 1. List of Simplification Assumptions

Field	Assumptions	Effects
Hydrodynamics	1. No solids in the bubble (void) phase 2. No net gas flow through emulsion phase 3. CSTR for solid flow pattern in both the dense bed and freeboard	1. No coke burning in the bubble (void) phase 2. All gas enters and leaves the bed as bubbles (voids) 3. Uniform carbon content and temperature distribution throughout these two regions
Reactions and kinetics	1. Instant combustion of hydrogen content 2. Fixed CO_2/CO for a modeled FCC regenerator	The complex regeneration reactions are simplified
Regenerator geometry	1. No transitional section between the dense bed and freeboard 2. The height of dense bed is always equal to the bottom section height of smaller diameter	The computation of the axial solid concentration profiles is simplified

are calculated by the carbon balance module. If $C_{Cd0} \neq C_{Cd1}$ and $C_{Cf0} \neq C_{Cf1}$, C_{Cd} and C_{Cd} are set to other initial values, and the gas component balance and carbon balance modules are executed again. With this inner loop, C_{Cd} and C_{Cd} are determined. After the determination of C_{Cd} and C_{Cd}, new values of T_d and T_f are calculated by the heat balance module. Similarly, with this outside loop, T_d and T_f are determined. Finally, the modeled results are printed by the output module.

During the modeling, there are some other basic parameters needed. The methods to setting or computing their values are listed in Table 2.[37,38]

Model Validation and Discussion

Model validation

Industrial data[39] from a FCC unit in Luoyang Petrochemical Corporation, Sinopec, China were used to validate this regenerator model. This FCC unit has a coaxial reactor-regenerator layout, processing 1.4 million tons of atmospheric residue per year. The catalyst used in this unit was a type of USY zeolite catalyst, whose measured kinetics constants k_{C0} and E_C as expressed in Eq. 7 were 2.967 $(Pa{\cdot}s)^{-1}$ and 1.422×10^5 kJ/kmol, respectively.[40,41] A single-stage countercurrent regenerator was used to regenerate the spent catalyst. This regenerator was first operated in full CO combustion mode with CO promoter used. Later, to increase the processing capacity and decrease the main air flow rate, the regenerator was revamped to partial CO combustion mode with reduced air flow rate and without CO promoter. Here, the full CO combustion mode refers to a FCC regeneration process where redundant oxygen is provided, characterized by high oxygen concentrations in the flue gas, whereas the partial CO combustion mode refers to a FCC regeneration process where less amount of oxygen is provided, characterized by low oxygen concentration in the flue gas. To keep appropriate regeneration performance under the partial CO combustion mode, a spent catalyst distributor was used to improve the catalyst distribution, and the catalyst inventory was increased to prolong the reaction time.

The advantage of this model is that only one fitting parameter, i.e., the interchanging solid flux between the dense bed and the freeboard, $F_{s,df}$, is used. In the process to determine the unit-dependent parameters, the partial CO combustion mode was first modeled. $F_{s,df}$ was determined based on the temperature difference in the dense bed and freeboard in the industrial unit. With this same value of $F_{s,df}$, the full CO combustion mode was then modeled. The modeled results for both partial and full CO combustion modes are compared with industrial data in Table 3. The main modeled hydrodynamic and performance results are in reasonable agreement with the industrial data, demonstrating the feasibility of this model. Moreover, these two regeneration modes are modeled with the same model parameter, showing the robustness of this model.

Discussion of model results

Profiles of Main Hydrodynamic and Reaction Parameters. With the current model, the axial profiles of voidage, temperature, gas components, and carbon content can be predicted, as shown in Figures 9 and 10 for partial and full CO combustion modes, respectively. In Figures 9a and 10a, it can be seen that most of the solid inventory in the freeboard is concentrated in the zone between the bed surface and ~ 2 m higher, where solid mixing is vigorous and a large solid exchange flux exists between the dense bed and the freeboard. Therefore, there are only small temperature increases in the freeboard, as seen in Figures 9b and 10b.

In Figures 9c and 10c, steep decreases in oxygen concentrations are predicted in the bubble phase and steep increases in steam concentration at the bed surface. This is attributed to the assumption of instant combustion of hydrogen at the bed surface. Because of the different mass-transfer rates, the concentration profiles of gas components follow different trends in the grid and bubbling zones. As seen in Figure 11, oxygen contents in the dilute phase of the grid zone decrease faster than in the bubbling zone. In the grid zone, oxygen concentrations in the emulsion phase are just a little lower than the corresponding oxygen concentrations in the dilute phase. However, in the bubbling zone, oxygen concentrations in the emulsion phase are much lower than the corresponding oxygen concentrations in the dilute phase and also much lower than the emulsion-phase oxygen concentrations in the grid zone. Table 4 lists the mass-transfer and reaction constants in bubbling and grid zones. It can be seen that mass-transfer constants in the grid zone are far greater than the corresponding reaction constants in both regeneration modes, showing that reaction kinetics is the controlling factor here. For the partial CO combustion mode, the reaction

Table 2. Model Parameters

Parameter	Equation	References
μ_g	$\mu_g = 18.27 \times 10^{-6} \cdot \frac{T_N+120}{T+120} \cdot \left(\frac{T}{T_N}\right)^{3/2}$	Chapman–Enskog equation[37]
C_{pg}	$C_{Pg} = 0.927 + 2 \times 1.279 \times 10^{-4} T - 1.28 \times 10^{-8} (2T)^2$	38
C_{ps}	$C_{ps} = 1.097$ kJ/(kg K)	
ΔH_{CO_2}	$\Delta H_{CO_2} = 33{,}873$ kJ/kg	33
ΔH_{CO}	$\Delta H_{CO} = 10{,}258$ kJ/kg	
ΔH_{H_2O}	$\Delta H_{H_2O} = 119{,}890$ kJ/kg	

Table 3. Comparison between Model Predictions and Industrial Data

Items		Partial Mode		Full Mode	
Flow rate of main air (m^3/min)		2988		3186	
Diameter of dense bed (m)		9.9		9.9	
Diameter of freeboard (m)		13.1		13.1	
Catalyst inventory (ton)		185		160	
Superficial gas velocity in the dense bed (m/s)		0.85		0.93	
Superficial gas velocity in the freeboard (m/s)		0.48		0.52	
Items for Comparison		Model	Exp.	Model	Exp.
Bed height of dense bed (m)		7.91		8.05	
Bed density (kg/m^3)		278	276	221	220
Freeboard density (kg/m^3)		10.9	12	14.9	14
Dense bed temperature (°C)		660	662	689	690
Freeboard temperature (°C)		669	670	696	699
Carbon content of the spent catalyst (wt %)		1.49		1.74	
Carbon content of the regenerated catalyst (wt %)		0.18	0.15	0.038	0.05
CBI [kg/(h·ton (cat.))]		102.1	105.7	112.8	106.7
Components of flue gas (dry)(vol %)	O_2	0.89	0.8	3.31	3.1
	CO	1.61	1.6	0.31	0.3
	CO_2	16.88	16.8	15.8	15.4

constant is more than five times the mass-transfer constant in the bubbling zone, showing that mass transfer is the controlling factor. However, for the full CO combustion mode, the reaction constant is just a little larger than the mass-transfer constant, indicating that both are important. This is largely due to the very low carbon content.

As there is residual oxygen in the freeboard for both partial and full CO combustion modes, as seen in Figures 9c and 10c, the carbon content decreases slightly in the freeboard as shown in Figures 9d and 10d. The difference of carbon content between the dense bed and the freeboard depends on both the oxygen concentration in the freeboard and the interchange solid flux between the dense bed and freeboard, as can be seen in Eq. 46. The higher the oxygen content in the freeboard, the more the carbon combusted in the freeboard and the lower the carbon content in the freeboard. Otherwise, the higher the $F_{s,\,df}$, the higher the carbon content in the freeboard.

Effect of the Solid Exchange Flux Between the Dense Bed and Freeboard. As the only adjustable model parameter in this model, the solid exchange flux between the dense bed and freeboard, $F_{s,df}$, should be between the solid flux in the cyclone diplegs and the initial solid ejection flux at the bed surface estimated by

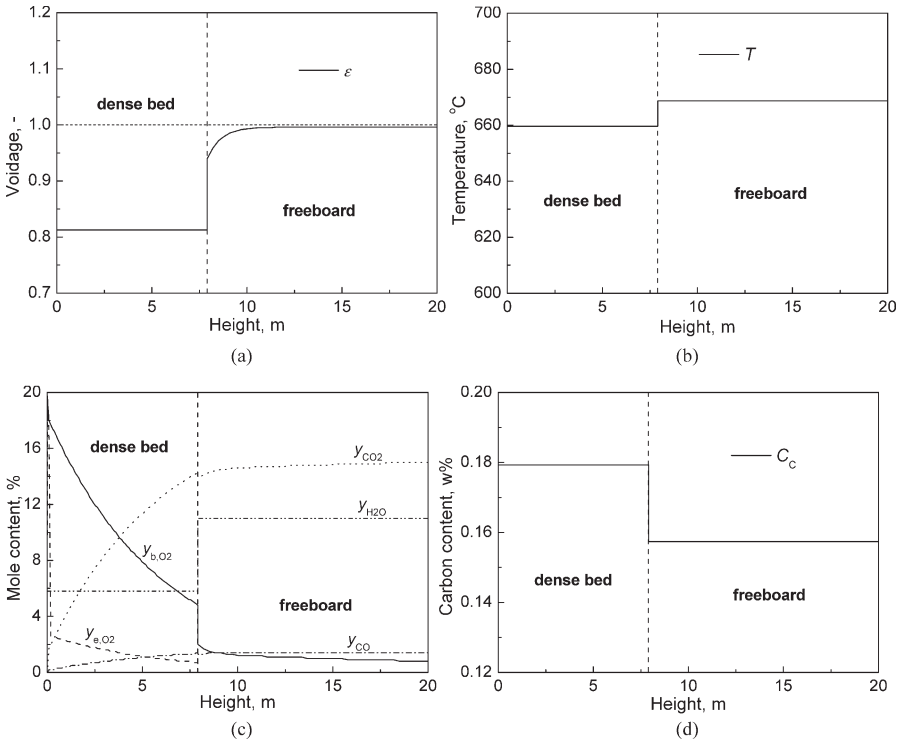

Figure 9. Predicted profiles of (a) voidage, (b) temperature, (c) gas composition, and (d) carbon content under partial CO combustion mode.

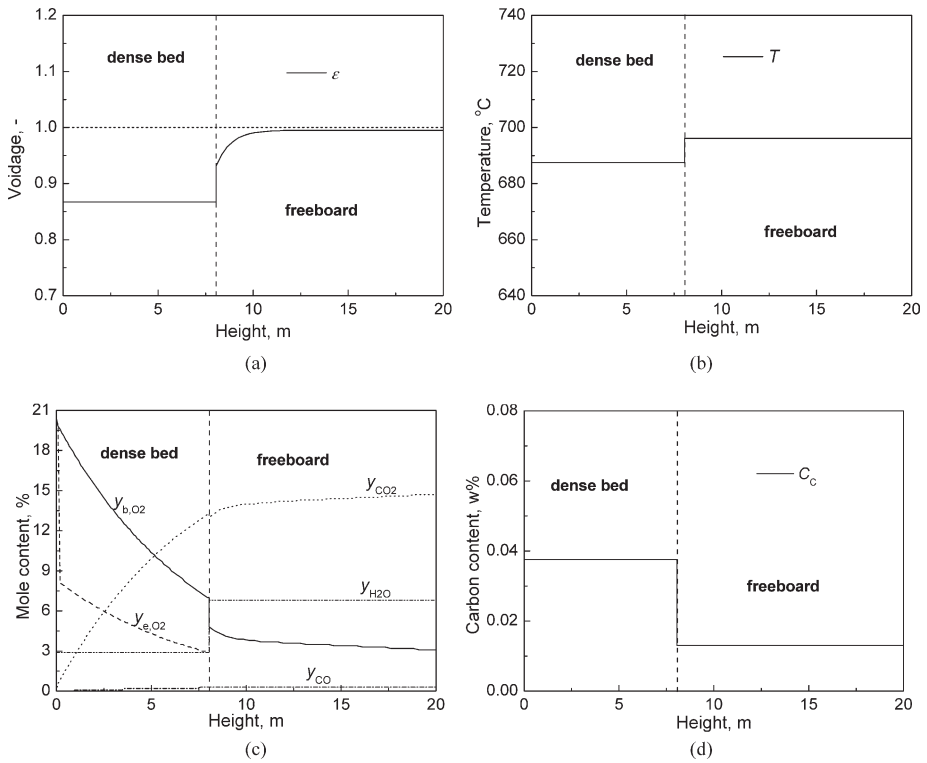

Figure 10. Predicted profiles of (a) voidage, (b) temperature, (c) gas composition, and (d) carbon content under full CO combustion mode.

$$F_{s,H_f} = 0.15\rho_p(u_1 - u_{mf})(1 - \varepsilon_{mf})A_{t1} \quad (65)$$

which follows the same method to determine the initial solid fraction at the bed surface in Eq. 19. In this model, the fitted $F_{s,df}$ is 24% of F_{s,H_f} and about five times the solid flux in the cyclone diplegs. With other parameters unchanged, the increase of $F_{s,df}$ increases the carbon content in the freeboard, thus increasing the carbon combustion rate. However, the predicted temperature difference between the dense bed and freeboard decreases accordingly. The decrease of $F_{s,df}$ decreases the carbon content and carbon combustion rate in the freeboard, but there is a higher temperature increase in the freeboard because of more heat absorbed by the freeboard particles.

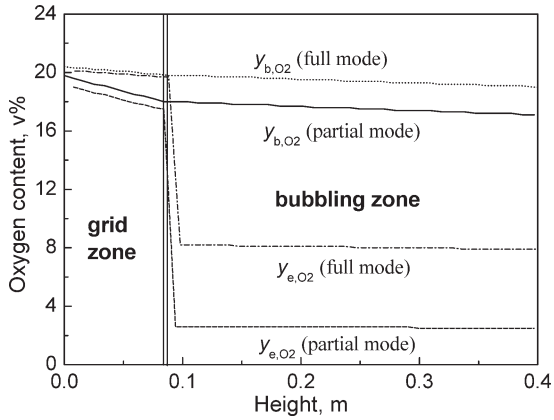

Figure 11. Oxygen concentration profiles in the grid and bubbling zones.

End Effects. The predicted results by this model also emphasize the importance of end effects, i.e., the effects of the grid zone and freeboard, on the regenerator performance. Table 5 compares the inventory fractions, fractions of carbon combusted, and the CBIs in the grid zone, bubbling zone, and freeboard. For the partial CO combustion mode, the fraction of carbon combusted in the grid zone can reach 10.9%, and the CBI is more than 10 times that in the bubbling zone, although it takes only less than 1.0% of the whole solid inventory. The effect of freeboard should not be neglected either, because the freeboard has a considerable solid inventory. Although the CBI in the freeboard is relatively small because of the low oxygen concentration, the freeboard is still predicted to combust 8% of the whole carbon. For the full CO combustion mode, the CBI in the grid zone is also far greater than in the bubbling zone in spite of the lower carbon content. Because of the higher superficial gas velocity, more particles are entrained into the freeboard. With the help of high oxygen content, the freeboard is predicted to contribute more than 11.7% of the carbon combustion.

Table 4. Comparison of Reaction and Mass-Transfer Constants

	Partial Mode		Full Mode	
	Grid Zone	Bubbling Zone	Grid Zone	Bubbling Zone
Mass-transfer constant (s^{-1})	29.9	0.17	32.3	0.21
Reaction constant (s^{-1})	0.97	0.97	0.30	0.30

Table 5. Effect of Grid, Bubbling, and Freeboard Zones on Regeneration Performance

	Zone	Grid	Bubbling	Freeboard
Partial mode	Inventory fraction (%)	0.96	89.38	9.66
	Fraction of carbon combusted (%)	10.87	81.3	7.83
	CBI [kg/(h ton (cat.))]	1097	84.8	78.5
Full mode	Inventory fraction (%)	0.93	83.9	15.16
	Fraction of carbon combusted (%)	3.66	84.66	11.67
	CBI [kg/(h ton (cat.))]	427	97.1	83.2

In summary, the end effects must be considered in modeling FCC regenerators. Moreover, more efforts are needed in designing the distributors of FCC regenerators, especially those under the partial CO combustion mode.

Effects of Air Flow Rate, Solid Inventory, and Pressure. With this model, the effects of main operating parameters, such as air flow rate, solid inventory, and operating pressure, on regeneration performance can be investigated. This helps to optimize the operation of FCC regenerators. Figure 12 shows the change of carbon content in regenerated catalysts, C_{Cr}, with air flow rate, solid inventory, and operating pressure changing within a $\pm 30\%$ range.

The air flow rate has the most important effect on C_{Cr}, as seen in Figures 12a1, b1. As the air flow increases, C_{Cr} is predicted to decrease because of the increase of oxygen concentration, mass-transfer rate, and carbon combustion rate. At a small air flow rate, an increase of air flow results in a very pronounced reduction in C_{Cr}. However, at a high air flow rate, only very small reduction of C_{Cr} can be achieved by increasing the air flow rate. With decreasing C_{Cr}, the global regeneration shifts gradually from mass-transfer-control to reaction-kinetics-control.

Solid inventory is predicted to have a smaller effect on C_{Cr}, as seen in Figures 12a2, b2. Solid inventory determines

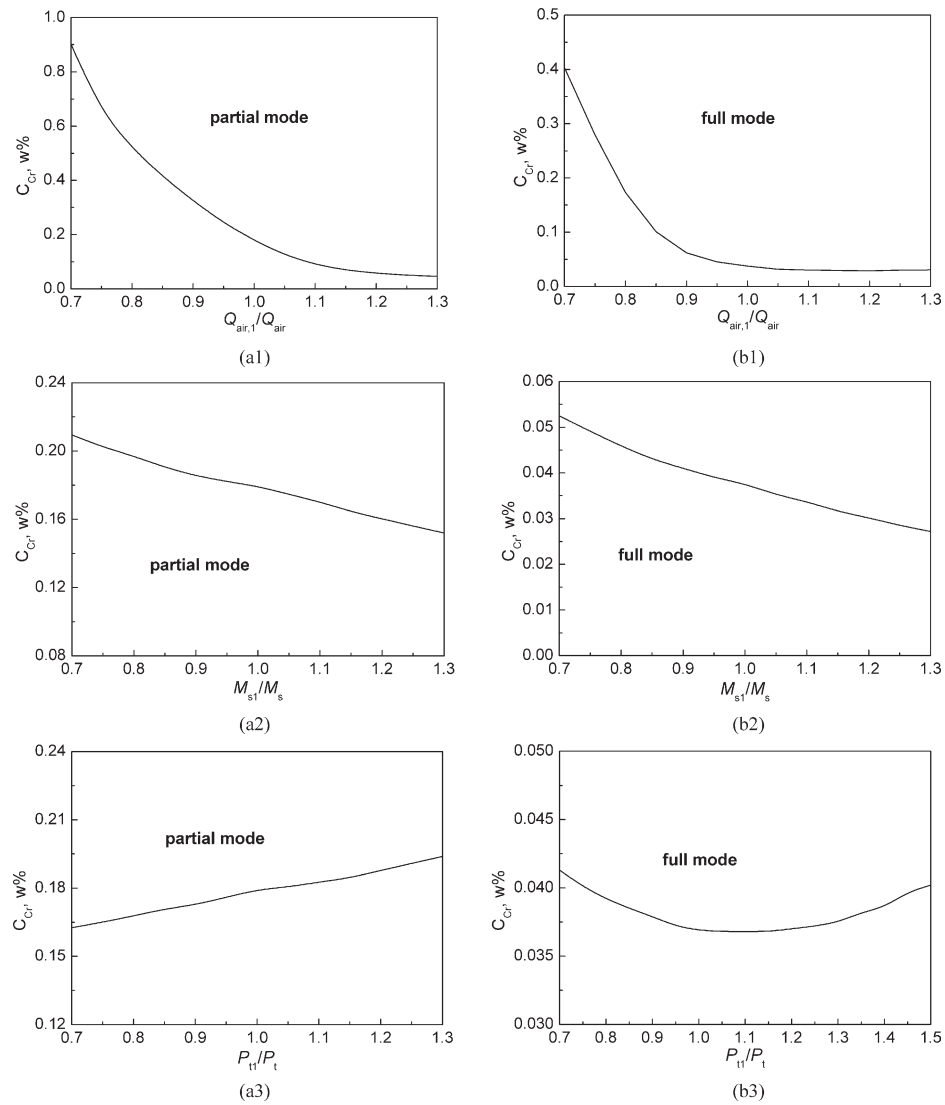

Figure 12. Effects of air flow rate (a1, b1), solid inventory (a2, b2), and operating pressure (a3, b3) on carbon content in the regenerated catalysts under partial and full combustion modes.

the average residence time of solid or the average reaction time. As solid inventory increases, C_{Cr} decreases steadily. Increase in solid inventory contributes to a larger reduction in C_{Cr} for the partial CO combustion mode than for the full CO combustion mode. On the other hand, it is shown that it is better to increase catalyst inventory than air flow rate to achieve a lower C_{Cr} for the full CO combustion mode, as reaction kinetics plays a more important role than under the partial CO combustion mode.

Increasing pressure can increase oxygen partial pressure and thus increase the carbon combustion rate. However, superficial gas velocity is reduced, as is the predicted reduced interphase mass-transfer rate. As shown in Figures 12a3, b3, the effects of pressure on C_{Cr} are different for the partial and full CO combustion modes. Under partial CO combustion mode, C_{Cr} is predicted to increase with increasing pressure, showing that interphase mass transfer plays a more important role. Under full CO combustion mode, there is little effect of pressure on C_{Cr}. However, it seems from Figures 12b3 that oxygen pressure may dominate when $P_{t1}/P_t < 1.1$, and interphase mass transfer may dominate when $P_{t1}/P_t = 1.1$.

The above sensitivity analysis serves not only as model validation tools. The results can also help and guide FCC operators to optimize the operations of FCC regenerators. For example, if they want to reduce the C_{Cr} while the regenerator is operated in partial CO combustion mode, the most effective measure is to increase the main air rate. However, the effect diminishes as main air rate increases. There exists a critical value beyond which increasing main air rate becomes poorly effective. In this study, the critical main air rate is near 1.1 times of its original air rate. Here, increasing solid inventory, i.e., prolonging the solid residence time, is more effective. If the regenerator is operated in full CO combustion mode, further increase of main air rate is almost useless. Increasing solid inventory seems to be a better choice. Comparatively, the effect of adjusting operating pressure is least effective.

Conclusions

A practical countercurrent FCC regenerator model was proposed with improved descriptions of gas and solid flow patterns. A three-zone and two-phase gas model was utilized to describe the gas flow through the regenerator, addressing the different phase mass-transfer properties in the different zones. A new two-CSTR-with-interchange model was used to describe the solid flow and to address the effect of freeboard on catalyst regeneration. Otherwise, this model also considered the expanding section usually used in a FCC regenerator to reduce solid carryover. The model was programmed in Matlab language with coupled mass and heat balances and coupled hydrodynamics and reaction kinetics. After validating and analysis of the effects of main influencing factors, the following conclusion can be drawn:

(1) After tested and validated based on the data from an industrial FCC regenerator operated under both partial and full CO combustion modes, the modeled results could be in reasonable agreement with the commercial data for both modes.

(2) There is only one fitting parameter, i.e., the interchange solid flux between the dense bed and freeboard, F_{s,H_f}. In this study, the fitted F_{s,H_f} in partial CO combustion mode can also be applicable in full CO combustion mode, showing the robustness of this model.

(3) In both partial and full CO combustion modes, reaction kinetics is the controlling factor for coke burning in the grid zone because of the very high interphase mass-transfer rate there. In the bubbling zone, mass transfer is the controlling factor for partial CO combustion mode, but both mass transfer and reaction kinetics can be comparatively important for full CO combustion mode because of the low carbon content in catalyst.

(4) Grid zone and freeboard are both predicted to have significant effects on catalyst regeneration because of their high interphase mass-transfer rate and large solid volume fraction, respectively, further demonstrating that they must be considered in FCC regenerator modeling.

(5) In partial CO combustion mode, the most effective measure to reduce the C_{Cr} is to increase the main air rate. However, the effect diminishes as main air rate increases. There exists a critical value beyond which increasing main air rate becomes poorly effective. To reduce the C_{Cr} in full CO combustion mode, increasing main air rate is almost useless and increasing solid inventory is a better choice.

Acknowledgments

The authors acknowledge the financial supports from the National Natural Science Foundation of China (Grant nos. 20906101 and 20976190), the Ministry of Science and Technology of China (Grant no. 2012CB215004) and the Chinese Scholarship Council. The authors also thank Dr. John R. Grace and Dr. Xiaotao Bi in University of British Columbia, Canada, for their precious advices and patient revision in writing this article.

Notation

A_j = cross-sectional area of jet, m^2
A_{t1}, A_{t2} = cross-sectional area of dense bed and freeboard, m^2
Ar = Archimedes number, $d_p^3\rho_g(\rho_s - \rho_g)g/\mu_g^2$, dimensionless
B_{Cd} = constant of heat flux in dense bed, kJ/(K s)
B_{Cf} = constant of heat flux in freeboard, kJ/(K s)
C_{Ab}, C_{Ae} = concentrations of gas component A in bubble and emulsion phase, vol %
CBI = coke burning intensity, kg/(ton·h)
C_C = carbon content, wt %
C_{Cd}, C_{Cf} = carbon contents in the dense bed and freeboard, wt %
C_{Cd0}, C_{Cf0} = initial values of carbon contents in the dense bed and freeboard, wt %
C_{Cd1}, C_{Cf1} = computed values of carbon contents in the dense bed and freeboard from initial values, wt %
C_{Cr} = carbon content in the regenerated catalyst, wt %
C_{Cs} = carbon content in the spent catalyst, wt %
C_{Hs} = hydrogen content in the spent catalyst, wt %
C_{pg} = specific heat of gas, kJ/(K·kg)
C_{ps} = specific heat of solid, kJ/(K·kg)
CBI = coke burning intensity, kg/(h·ton)
d_{or} = orifice diameter, m
d_p = particle mean diameter, m
d_t = column diameter, m
d_{t1}, d_{t2} = column diameters of the dense bed and freeboard, m
$D_{a,s}$ = solid axial dispersion coefficient, m^2/s
D_j = jet diameter, m
E_C = activation energy for carbon combustion, kJ/kmol
f_s = solid fraction, dimensionless
f_s^0 = initial solid fraction of freeboard, dimensionless
f_s^* = saturated solid fraction of freeboard, dimensionless
f_{sb} = solid fraction in bubble phase, dimensionless
f_{se} = solid fraction in emulsion phase, dimensionless
F_{s0} = catalyst circulation rate between reactor and regenerator, kg/s
$F_{s,df}$ = catalyst circulation rate between dense bed and freeboard, kg/s
F_{s,H_f} = initial solid ejection flux at bed surface, kg/s
g = gravitational acceleration, m/s
G = parameter, dimensionless
h = height, m

H_f = expanded bed height, m
H_L = height of freeboard, m
H_t = total height of column, $H_t = H_f + H_L$, m
k_{be} = interphase mass-transfer coefficient, m/s
k_C = carbon combustion rate coefficient, 1/(Pa s)
k_{C0} = pre-exponent for k_C
k_j = interphase mass-transfer coefficient, kg/m^2 s
k_r = reaction constant in Eqs. 2 and 3, s^{-1}
K_{be} = interphase mass-transfer coefficient, s^{-1}
K_{db} = mass-transfer constant in bubbling zone of dense bed, s^{-1}
K_{dj} = mass-transfer constant in the grid zone of dense bed, s^{-1}
K_{dr} = reaction constant in dense bed, s^{-1}
K_{fr} = reaction constant in freeboard, s^{-1}
L_j = jet length or grid zone height, m
Ly = Lysenko number, $Ly = u_0^3\rho_g^2/(\rho_p - \rho_g)\mu_g g$, dimensionless
M_d = solid inventory in dense bed, kg
M_f = solid inventory in freeboard, kg
M_s = total solid inventory in the regenerator, kg
$M_{s'}$ = changed total solid inventory in the regenerator, kg
M_A = molar mass of air, kg/mol
n = power index of Eq. 12, dimensionless
N = number of CSTRs for tank-in-series model, dimensionless
N_j = gas molar flow rate per orifice, kmol/s
N_{dt} = total gas molar flow rate in dense bed, kmol/s
N_{ft} = total gas molar flow rate in freeboard, kmol/s
P_d, P_f = pressure in the dense bed and freeboard, Pa
P_N, = pressure at normal condition, 1.013×10^5 Pa
P_{O2} = partial pressure of oxygen, Pa
P_t = pressure in the top of a FCC regenerator, Pa
P_{t1} = changed pressure in the top of a FCC regenerator, Pa
Pe_s = solid Peclet Number, $Pe_s = \frac{u_s H_f}{D_{a,s}}$, dimensionless
Q_{air} = volume flow rate of main air, m^3/s
$Q_{air,1}$ = changed volume flow rate of main air, m^3/s
Q_{Cd} = heat flux constant in dense bed, kJ/s
Q_{Cf} = heat flux constant in freeboard, kJ/s
Q_{dc} = heat release flux due to catalyst coolers in dense bed, kJ/s
Q_{dd} = heat flux of coke desorption in dense bed, kJ/s
Q_{d1} = heat releasing flux due to outside shell of dense bed, kJ/s
Q_{dr1} = heat released due to combustion of carbon in dense bed, kJ/s
Q_{dr2} = heat released due to combustion of hydrogen in dense bed, kJ/s
Q_{fd} = coke desorption heat flux in freeboard, kJ/s
Q_{f1} = heat releasing flux due to outside shell of freeboard, kJ/s
Q_{fr1} = heat released due to combustion of carbon in freeboard, kJ/s
Q_{fr2} = heat released due to combustion of hydrogen in freeboard, kJ/s
r_{Cd}, r_{Cd} = carbon loss rates due to combustion in the dense bed and freeboard, kg/s
R = gas law constant (8.306), kJ/(kmol·K)
T = temperature, K
T_N = temperature at normal condition, 273.15 K
T_0 = temperature of main air, K
T_d, T_f = temperatures in the dense bed and freeboard, K
T_{d0}, T_{f0} = initial values of temperatures in the dense bed and freeboard, K
T_{d1}, T_{f1} = computed values of temperatures in the dense bed and freeboard for initial values, K
T_N = temperature at standard condition, 273.16 K
T_s = temperature of spent catalysts, K
u_0 = superficial gas velocity, m/s
u_1, u_2 = gas velocities in the dense bed and freeboard of a FCC regenerator, m/s
u_{1e}, u_{2e} = measured gas velocities in the dense bed and freeboard of a FCC regenerator, m/s
u_b = bubble rise velocity, m/s
u_{mf} = minimum fluidization velocity, m/s
u_{or} = gas ejection velocity from distributor orifices, m/s
u_{H_2O} = addition gas flow rate increase due to combustion of hydrogen in coke, m/s
u_s = superficial solid velocity, m/s
V_{md} = molar volume in dense bed, m^3/kmol
V_{mf} = molar volume in freeboard, m^3/kmol
y_{CO_2}, y_{CO}, y_{H_2O}, y_{O_2} = mole fractions of CO_2, CO, H_2O, and O_2, dimensionless
y_{b,O_2}, y_{e,O_2} = mole fractions of O_2 in the bubble (jet) and emulsion phases of the dense bed, dimensionless
y_{f,CO_2}, $y_{f,CO}$, y_{f,H_2O}, y_{f,O_2} = mole fractions of CO_2, CO, H_2O, and O_2 in flue gas, dimensionless
z = height, m
z_f = distance above dense bed surface, m

Greek letters

α = coefficient of Eq. 17, m^{-1}
α_b = interphase area per volume of bubble, m^2/m^3
α_{ji} = interphase area per volume of jet, m^2/m^3
β = CO_2/CO, dimensionless
δ_b = bubble volume fraction, dimensionless
ΔH_{CO} = heat released per kilogram of carbon combusted into CO, kJ/kg
ΔH_{CO_2} = heat released per kilogram of carbon combusted into CO_2, kJ/kg
ΔH_{H_2O} = heat released per kg of hydrogen combusted into H_2O, kJ/kg
ε = voidage, dimensionless
ε_B = average bed voidage, dimensionless
ε_{mf} = voidage at minimum fluidization velocity, dimensionless
μ_g = gas viscosity, Pa s
$\varepsilon_{g,j}$ = gas viscosity in jets, Pa s
π = circumference ratio (3.14), dimensionless
ρ_B = apparent bed density, kg/m^3
$\rho_{B,exp}$ = measured bed density, kg/m^3
ρ_f = particle concentration in the freeboard, kg/m^3
ρ_g = gas density, kg/m^3
$\rho_{g,j}$ = gas density in jets, kg/m^3
ρ_{in} = measured solid concentration in the cyclone inlet, kg/m^3
ρ_p = particle density, kg/m^3

Subscripts

b = bubble phase
B = bed
d = dense bed
e = emulsion phase
f = freeboard
ex = exit
exp = experiment
f = freeboard
g = gas
in = inlet
j = jet
mf = minimum fluidization
or = orifice
p = particle
s = solid

Literature Cited

1. Shan H, Li C, Niu G, Yang C, Zhang J. Research progress in fluid catalytic cracking technology. *J Univ Pet China*. 2005;29:135–150(in Chinese).
2. Hemler CL, Smith LF. *UOP fluid catalytic cracking process*. In: Meyers RA, editor. *Handbook of Petroleum Refining Processes, Chapter 3.3*. New York, USA: McGraw-Hill, 2004. 3.47–3.69.
3. Ford FD, Reinmen RC, Vasalos IA, Fahrig RJ. Operating cat crackers for maximum profit. *Chem Eng Prog*. 1977;73:92.
4. De Lasa HI, Grace JR. The influence of the freeboard region in a fluidized bed catalytic cracking regenerator. *AIChE J*. 1979;25:984–991.
5. Errazu AF, De Lasa HI, Sarti F. A fluidized bed catalytic cracking regenerator model. *Can J Chem Eng*. 1979;57:191–197.
6. De Lasa HI, Errazu A, Barreiro E, Solioz S. Analysis of fluidized bed catalytic cracking regenerator models in an industrial scale unit. *Can J Chem Eng*. 1981;59:549–553.
7. Orcutt JC, Davidson JF, Pigford RL. Reaction time distributions in fluidized catalytic reactors. *Chem Eng Prog Symp Ser*. 1962;58:1–15.

8. Faltsi-Saravelou O, Vasalos IA, Dimogiorgas G. FBSim: a model for fluidized bed simulation. II. Simulation of an industrial fluidized catalytic cracking regenerator. *Comput Chem Eng*. 1991;15:647–656.
9. Filho RM, Batista LMFL, Fusco M. 1996. A fast fluidized bed reactor for industrial FCC regenerator. *Chem Eng Sci*. 1996;51:1807–1816.
10. Lu C. Study on the flow behavior in the FCC turbulent fluidized beds. Doctoral dissertation, China University of Petroleum, Beijing, China, 1996 (in Chinese).
11. Behie LA, Kehoe P. The grid region in a fluidized bed reactor. *AIChE J*. 1973;19:1070–1072.
12. Chavarie C, Grace JR. Performance analysis of a fluidized bed reactor. *Ind Eng Chem Fundam*. 1975;14:75–91.
13. Guigon P, Large JF, Bergougnou MA. Application of the Kunii-Levenspiel model to a multistage baffled catalytic cracking regenerator. *Chem Eng J*. 1984;28:131–138.
14. Lee LS, Yu SW, Cheng CT, Pan WY. Fluidized-bed catalyst cracking regenerator modeling and analysis. *Chem Eng J*. 1989;40:71–82.
15. Kunii D, Levenspiel O. *Fluidization Engineering*. New York, USA: Wiley, 1969.
16. McFarlane RC, Reineman RC, Bartee JF, Georgakis C. Dynamic simulator for a model IV fluid catalytic cracking unit. *Comput Chem Eng*. 1993;17:275–300.
17. Han LS, Chung CB. Dynamic modeling and simulation of a fluidized catalytic cracking process. I. Process modeling. *Chem Eng Sci*. 2010;56:1951–1971.
18. Han LS, Chung CB. Dynamic modeling and simulation of a fluidized catalytic cracking process. II. Property estimation and simulation. *Chem Eng Sci*. 2010;56:1973–1990.
19. Elnashaie SSEH, Mohamed NF, Kamal M. Simulation and static bifurcation behavior of industrial FCC units. *Chem Eng Commun*. 2004;191:813–831.
20. Fernandes JL, Verstraete J, Pinheiro CIC, Oliveira NMC, Ribeiro FR. Dynamic modeling of an industrial R2R FCC unit. *Chem Eng Sci*. 2007;62:1184–1198.
21. Schwarz MP, Lee J. Reactive CFD simulation of an FCC regenerator. *Asia-Pac J Chem Eng*. 2007;2:347–354.
22. Cao B, Zhang P, Zheng X, Xu C, Gao J. Numerical simulation of hydrodynamics and coke combustions in FCC regenerator. *Pet Sci Technol*. 2008;26:256–269.
23. Wang J, Van der Hoef MA, Kuipers JAM. Why the two-fluid model fails to predict the bed expansion characteristics of Geldart A particles in gas-fluidized beds: a tentative answer. *Chem Eng Sci*. 2009:64:622–625.
24. Grace JR, Taghipour F. Verification and validation of CFD models and dynamic similarity for fluidized beds. *Powder Technol*. 2004;139:99–110.
25. van Deemter JJ. *Mixing patterns in large-scale fluidized beds*. In: Grace JR, Masten JM, editors. *Fluidization*. New York, USA: Plenum Press, 1980:69–89.
26. Fogler HS. *Elements of Chemical Reaction Engineering*, 2nd ed. New Jersey: Prentice-Hall, 1992:781.
27. Levy EK, Caram HS, Dille JC, Edelstein S. Mechanisms for solids-ejection from gas-fluidized beds. *AIChE J*. 1983;29:383–388.
28. Wang G, Lin S, Yang G. Kinetics of combustion of carbon and hydrogen in carbonaceous deposits on zeolite-type cracking catalysts. *Ind Eng Chem Proc Des Dev*. 1986;25:626.
29. Arthur JR. Reactions between carbon and oxygen. *Trans Faraday Soc*. 1951;47:164–178.
30. Liu W, Li Z, Zhao X. Study on kinetics of regeneration of coke-deposited Y-15 cracking catalyst. *ACTA Pet Sin. (Pet Process Sect.)* 1995;11:36 (in Chinese).
31. Yan Q, Peng Y, Cheng Z, Yu F. Study on CO_2/CO ratio in product gas of spent catalytic cracking catalyst during regeneration. *Pet Process Petrochem*. 2001;32:56–58 (in Chinese).
32. Wu Z, Zhang J, Wang X. The effect of temperature and oxygen pressure on the CO content in FCC flue gas. *Pet Process Petrochem*. 2005;36:18–22 (in Chinese).
33. Cai P, Jin Y, Yu Z, Wang Z. Mechanism of flow regime transition from bubbling to turbulent fluidization. *AIChE J*. 1990;36:955–956.
34. Zhang Y, Lu C, Shi M. A practical method to estimate the bed height of a fluidized bed of FCC particles. *Chem Eng Tech*. 2008;31:1735–1742.
35. De Groot JH. *Scaling-up of gas-fluidized bed reactors*. In: Drinkenburg AAH, editor. *Proceeding of the International Symposium on Fluidization*. Amsterdam: Netherlands University Press, 1967:348–361.
36. Lin S. *Petroleum Refining Engineering*, 3rd ed. Beijing, China: Petroleum Industry Press, 2000 (in Chinese).
37. He L. *Subroutines for Chemical Process Calculations*. Beijing, China: China Petrochemical Press, 1993 (in Chinese).
38. Hirshfelder JO, Curtis CF, Bird RB. *Molecular Theory of Gases and Liquids*, 1st ed. New York, USA: Wiley, 1964.
39. Zhao Z, Liu J. Technical analysis of resid FCCU revamping from complete regeneration to incomplete regeneration. *Pet Process Petrochem*. 2001;32:14–18 (in Chinese).
40. Wei S. Dynamic criterion for regeneration of FCC catalyst. *Pet Refin Eng*. 2000;30:26–29 (in Chinese).
41. Dong X, Hao X. A technique to evaluate coke burning in FCC regenerator. *Pet Refin Eng*. 2006;36:7–9 (in Chinese).

Manuscript received July 10, 2011, and revision received Sept. 6, 2011.